ACS APPLIED MATERIALS & INTERFACES

Research Article

www.acsami.org

Facile Synthesis of Hierarchical Porous TiO_2 Ceramics with Enhanced Photocatalytic Performance for Micropolluted Pesticide Degradation

Zipeng Xing,[†] Wei Zhou,*[,†] Fan Du,[†] Linlin Zhang,[†] Zhenzi Li,[§] Hang Zhang,[†] and Wei Li*[,‡]

[†]Key Laboratory of Functional Inorganic Material Chemistry, Ministry of Education of the People's Republic of China, Key Laboratory of Chemical Engineering Process and Technology for High-Efficiency Conversion, College of Heilongjiang Province, Department of Environmental Science, Heilongjiang University, Harbin 150080, People's Republic of China

[‡]Department of Chemistry and Laboratory of Advanced Materials, Fudan University, Shanghai 200433, People's Republic of China

[§]Department of Epidemiology and Biostatistics, Harbin Medical University, Harbin 150086, People's Republic of China

Supporting Information

ABSTRACT: In this research, hierarchical porous TiO_2 ceramics were successfully synthesized through a camphene-based freeze-drying route. The well-dispersed TiO_2 slurries were first frozen and dried at room temperature, followed by high-temperature sintering. The ceramics were analyzed by X-ray diffraction, Raman spectroscopy, scanning electron microscopy, and transmission electron microscopy. Results indicated that the obtained TiO_2 ceramics could inhibit undesirable anatase-to-rutile phase transformation and grain growth even at temperatures as high as 800 °C. In this experiment, optimal compressive strength and porosity of the TiO_2 ceramics were produced with the initial TiO_2 slurry content of ~15 wt %. The resultant TiO_2 ceramics performed excellently in the photodegradation of atrazine and thiobencarb, and the total organic carbon removal efficiency was up to 95.7% and 96.7%, respectively. More importantly, the TiO_2 ceramics were easily recyclable. No obvious changes of the photocatalytic performance were observed after six cycles. Furthermore, the ceramics also effectively degraded other pesticides such as dimethoate, lindane, dipterex, malathion, and bentazone. These hierarchical porous TiO_2 ceramics have potential applications in environmental cleanup.

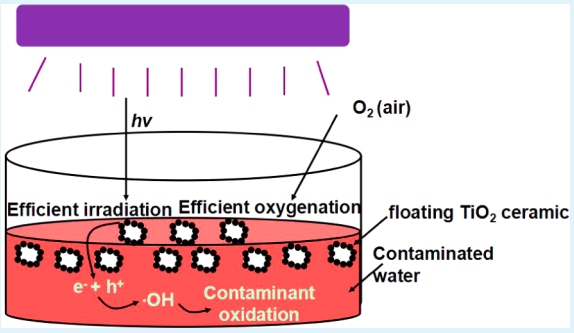

KEYWORDS: *porous TiO_2 ceramics, floating photocatalyst, room-temperature freeze-drying, photocatalysis, pesticide micropolluted water*

1. INTRODUCTION

Pesticides are one of the most notorious classes of organic pollutants due to their widespread use, toxicity, persistence, and bioaccumulation,[1,2] posing a great threat to environmental recipients. Some of these pollutants are biological refractory or inhibit organics, so it is very hard to degrade these pollutants by microorganisms naturally.[3] All currently available chemical oxidation techniques use either strong oxidizer or high-energy UV illumination, both risky and unsafe techniques.[4,5] They can form lots of intermediates during the processes, and owing to the low efficiency, the costs of the whole processes are quite expensive because of the complete destruction and mineralization of these intermediates. Consequently, industrial or natural water contained with these biological refractory and hazardous compounds needs advanced treatment processes.[6]

The heterogeneous photocatalytic technique is one of the most outstanding wastewater treatment technologies for the degradation of toxic pollutants.[7−10] In particular, TiO_2 semiconductor using as a heterogeneous photocatalyst can utilize low-energy UV light. It provides a potential possibility to exploit solar energy for contaminated water cleanup, so more focuses have been paid attention to this technology.[11] The utilization of solar light to remove pollutants means clean advantages from an environmental viewpoint.[12,13] Furthermore, it will possess the economic viability for the real application to compete with other water treatment techniques, for example, hydrogen peroxide/UV−C or ozone oxidation.[14]

However, three challenges have thus far prohibited the practical application of TiO_2: photoinduced electron−hole pair separating,[15−20] photon utilization improving,[21−24] and photocatalyst recycling.[25−28] Significant work has been dedicated to the issue, but at an industrial scale, more practical uses of this technology are needed.[29] Specifically, a facile and low-cost filtration step for high TiO_2 slurry concentrations must be provided before the TiO_2 particles can be applied.[30] To solve the problem of photocatalyst separation, immobilized TiO_2 particles on various larger carriers are studied.[31,32] However, an obvious drawback of these TiO_2-coated carriers detached the

Received: May 30, 2014
Accepted: September 8, 2014
Published: September 8, 2014

active TiO_2 particles gradually from the carrier surface through hydraulic blow and collision.[33] Furthermore, the intimate contact between light and photocatalysts will be in favor of enhancing photocatalytic efficiency. Floating photocatalysts have dramatic advantages due to the optimal light illumination process, particularly for a solar irradiation system, and the maximal oxygenation process based on their proximity to the air/water interface, particularly for a nonstirred system. It should result in increasing of the radical formation rate and oxidation efficiency.[34]

Owing to lightweight, large surface area, outstanding permeability, and high specific strength, open porous TiO_2 ceramics favor the diffusion and transfer of pollutants.[35] One growing interest is the freeze-drying (or freeze-casting) process as a facile, low-cost, and green synthetic technique for porous ceramic fabrication, which can tailor a designed pore distribution comparing to conventional techniques.[36−39] Three-dimensional interconnected pore channels can be formed when the frozen vehicle network is in the ceramic body. Especially concerning is that ceramic pore structure and size can be easily regulated by changing the processing parameters.[40] H_2O[41] and *tert*-butanol[42] have been successfully employed as frozen vehicles to fabricate porous ceramics. To avoid the expensive sub 0 °C freezing process, a new freeze-drying technique has currently been utilizing camphene ($C_{10}H_{16}$) as a frozen vehicle.[43] This method is safe, low-cost, and applicable near room temperature.[44]

In this paper, we design and fabricate lightweight porous crystalline TiO_2 ceramics as a floating photocatalyst by a camphene-based freeze-drying route for refractory pesticide micropolluted water degradation. Expanded vermiculite granules were added in the porous ceramics, which could give closed pores and retain the floatability of porous TiO_2 ceramic. Ethanediamine (EN)-modified Degussa P25 was used as the precursor to inhibit the anatase-to-rutile phase transformation of TiO_2 ceramic. Our former work had exhibited that the anatase TiO_2 phase could keep the high thermal stability up to 800 °C.[45,46] The effects of the slurry contents of porous TiO_2 ceramics were also investigated. These synthesized TiO_2 ceramics have both excellent mechanical strength and high photocatalytic performance. Finally, the application of the floating photocatalysts for refractory pesticide wastewater degradation was also examined.

2. EXPERIMENTAL SECTION

All reagents were of analytical grade, including atrazine, thiobencarb, dimethoate, lindane, dipterex, malathion, bentazone, EN, and polystyrene (PS). Camphene ($C_{10}H_{16}$) was used as the frozen vehicle, and Texaphor 963 was used as the dispersant. Expanded vermiculite granular was collected from Changbai Mountain (Jilin Province, China). Figure S1 (Supporting Information) showed a schematic of the preparation of porous TiO_2 ceramic. The different composition of TiO_2 ceramic slurries could be seen in Table 1. The specific synthesized method was depicted in our former works at length.[15,47] The carriers were changed for expanded vermiculites. The optimal freeze-drying time and high-temperature calcinations procedure were determined by thermal gravity analysis (Figure S2 A−D, Supporting Information). The final synthesized hierarchical porous TiO_2 ceramic could float on the wastewater well in Figure S3 (Supporting Information). The average 0.02 g of mass and Φ 1*0.2 cm of dimension was for one piece of TiO_2 ceramics (Figure S4, Supporting Information).

Table 1. Composition of TiO_2 Ceramic Slurries

component	EN-modified TiO_2	polystyrene	Texaphor 963	camphene	expanded vermiculite
weight (%)	10	0.6	0.6	78.6	10.2
weight (%)	15	0.6	0.6	74.1	9.7
weight (%)	20	0.5	0.5	69.9	9.1

The synthesized floating porous TiO_2 ceramic photocatalysts were analyzed by X-ray diffraction (XRD), Raman spectroscopy, scanning electron microscopy (SEM), transmission electron microscopy (TEM), nitrogen adsorption−desorption isotherms, mercury porosimetry (model pore sizer 9500, Micrometritics Co. Ltd., USA), the Archimedes method, and the compressive strength test referring to our former operation.[15,47] Total organic carbon (TOC) analysis was performed using a TOC-VCPN (Shimadzu, Japan) analyzer referring to the standard methods.[48]

Atrazine and thiobencarb have been considered as both potentially hazardous and carcinogenic. Therefore, they were determined as the model micropolluted pesticides to inspect the photocatalytic efficiency with the synthesized porous TiO_2 ceramic. After each photocatalytic process, the atrazine and thiobencarb concentrations were analyzed by TOC-VCPN. In addition, the mineralization ratios of dimethoate, lindane, dipterex, malathion, and bentazone were also tested by TOC-VCPN after a 2 h photocatalytic process. The detailed operational procedure and condition of the photocatalytic test also could be referred to our former reports.[15,47] The schematic representation of a floating porous TiO_2 ceramic for contaminants oxidation is shown in Figure S5 (Supporting Information).

3. RESULTS AND DISCUSSION

3.1. Structure and Characterization of Porous TiO_2 Ceramic. The crystalline phase of TiO_2 can significantly influence the photocatalytic performance.[49] Figure 1 exhibits

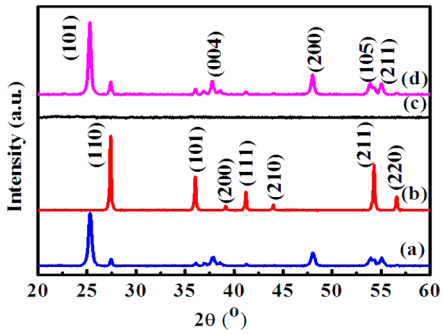

Figure 1. XRD patterns of (a) Degussa P25, (b) TiO_2 ceramic synthesized from Degussa P25 with 15 wt % TiO_2 solid content slurries at 800 °C, (c) expanded vermiculite, and (d) TiO_2 ceramic synthesized from EN-modified Degussa P25 with 15 wt % TiO_2 solid content slurries at 800 °C, respectively.

the XRD patterns of porous TiO_2 ceramics synthesized from Degussa P25 and EN-modified Degussa P25 with 15 wt % TiO_2 solid content slurries at 800 °C calcinations. In Figure 1a, d, five characteristic XRD peaks were found at 25.2°, 37.8°, 48.1°, 53.9°, and 56.1°, which can be ascribed to anatase TiO_2(101), (004), (200), (105), and (211), respectively. In Figure 1b, seven characteristic XRD peaks were found at 27.4°, 36.1°, 39.2°, 41.2°, 44.1°, 54.3°, and 56.6°, which can be ascribed to rutile TiO_2(110), (101), (200), (111), (210), (211), and (220), respectively. In addition, the intensity of the XRD peaks increased at 800 °C calcinations, indicating the higher anatase TiO_2 crystallinity. In Figure 1b, Degussa P25 was transformed into the rutile phase after being calcined at 800 °C, which was reasonable in that rutile TiO_2 was more thermodynamically

stable. Nevertheless, the EN-modified TiO_2 could still retain the anatase phase at 800 °C, suggesting that its thermal stability was excelled in previous reports.[50−54] In our former work,[46] we understand that EN could interact with Degussa P25 strongly and bind on the surface. It was also as an effective protector, capable of inhibiting the undesirable TiO_2 particle growth and crystal phase transformation. So, the strong alkaline EN having two primary amine groups and two positive charges would combine with the Degussa P25 strongly. Protected by the EN species, the TiO_2 nanoparticles could not contact directly, thereby improving anatase TiO_2 crystallinity and prohibiting the anatase-to-rutile phase transformation. By using the Scherrer formula to calculate the anatase (101) diffraction peaks, the average 22 nm of the Degussa P25 particle was obtained. After 800 °C calcinations, 48 and 23 nm of Degussa P25 and EN-modified Degussa P25 particles were obtained, respectively, demonstrating that the TiO_2 crystallite size was suppressed by surface EN modification, which would elevate the photocatalytic performance. In addition, 49.8 m^2/g of the specific Brunauer−Emmett−Teller (BET) surface area for EN-modified TiO_2 ceramic was observed (Figure S6, Supporting Information), which was close to Degussa P25 (~50 m^2/g). There was no obvious decrease, suggesting that the surface area of TiO_2 particles could be retained by EN protection, which was beneficial for photocatalysis.

Raman spectroscopy is a promising method to evaluate crystalline TiO_2. It selects a sampled area several micrometers in size and scans the samples surface to identify different Raman-active phases. Therefore, in order to further reveal phase transformation behavior and verify the high crystallinity of prepared porous TiO_2 ceramics, Raman characterization was conducted. Figure 2 showed the Raman spectra of porous TiO_2 ceramic with 15 wt % TiO_2 solid content slurries at 800 °C calcinations. In Figure 2a, d, five high intensity Raman peaks at 149, 199, 393, 513, and 639 cm^{-1} could be indexed to the E_g, E_g, B_{1g}, $A_{1g}(B_{1g})$, and E_g modes, respectively, which were the representation of the anatase TiO_2. Moreover, the intensity of the Raman peaks increased at 800 °C calcinations, indicating the higher TiO_2 anatase crystallinity, which was consistent with the XRD characterization. In Figure 2b, pure Degussa P25 ceramic was similarly transformed into the rutile phase calcinated at 800 °C, and four different Raman peaks at 143, 244, 442, and 609 cm^{-1} could be found and indexed to B_{1g}, the multiphoton process, E_g, and A_{1g} modes, respectively, which were the representation of the rutile TiO_2. It indicated that the TiO_2 anatase-to-rutile phase transformation was ongoing under this sintered temperature. All these showed the consistent results as well as the XRD analysis.

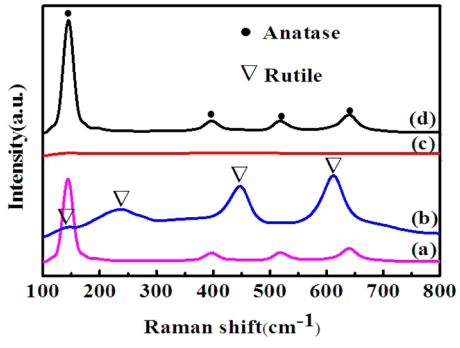

Figure 2. Raman spectra of (a) Degussa P25, (b) TiO_2 ceramic synthesized from Degussa P25 with 15 wt % TiO_2 solid content slurries at 800 °C, (c) expanded vermiculite, and (d) TiO_2 ceramic synthesized from EN-modified Degussa P25 with 15 wt % solid content slurries at 800 °C, respectively.

The microstructure evolution of sintered TiO_2 ceramic with 10, 15, and 20 wt % TiO_2 solid content slurries at 800 °C calcination was further observed by SEM characterization. These samples were denoted as W10, W15, and W20, respectively. Figure 3 indicated that the initial TiO_2 solid content significantly influenced the porous TiO_2 ceramic solid struts and its porosity. When the TiO_2 solid content raised, the TiO_2 ceramic solid struts were compacted (incompact bonded particles were found in Figure 3A, B, and yet, sintered solid struts were observed in Figure 3C−F). Moreover, a lot of fine pores were found in Figure 3A, B. As the TiO_2 solid content raised, these fine pores vanished gradually, as found by comparing Figure 3A and B to E and F. Schematic illustration of the camphene-based freeze-drying technique is shown in Figure 4. TiO_2 ceramic powders were homogeneously dispersed in the molten camphene solution by the warm ball-milling at 60 °C. After freeze-drying at room temperature, the molten camphene is frozen and grown dendritically at once, and meanwhile, the TiO_2 ceramic powders are expelled by the growing solid camphene and become condensed between the solid camphene dendrites. This freezing behavior forms a bicontinuous structure, that is, the separated solid camphene phase and condensed TiO_2 ceramic powder networks are interconnected in three-dimensional space. SEM observations revealed that a lower TiO_2 solid content brought a higher porosity. In addition, when initial TiO_2 solid content was raised, the pore sizes were smaller, and yet, the calcined TiO_2 solid walls were thicker. On the one hand, more TiO_2 nanoparticles would fill hollow spaces that could decrease the porosity and influence compressive strength. On the other hand, during freezing, the condensed TiO_2 concentration could create the capillary drag force in the solid/liquid interface, which could inhibit the growth of the solid camphene dendrites. Thus, it is reasonable to demonstrate that a higher TiO_2 solid content would result in forming the smaller camphene dendrites and the thicker condensed TiO_2 solid walls. Furthermore, the average 20−30 nm diameter of TiO_2 ceramic particles was observed.

The TiO_2 solid content is significant in influencing the porosity and mechanical strength of the calcined samples. From Figure 5, the different TiO_2 solid content acting the porosity and compressive strength was also studied. With increasing the TiO_2 solid content from 10 to 20 wt %, the porosity was 95.2%, 92.9%, and 89.6%, respectively, but the compressive strength raised from 0.59 to 0.98 MPa. When the TiO_2 solid content was raised, the lower porosity as well as the greater mechanical strength could be obtained. These results were in good agreement with the SEM analysis. It is well known that higher porosity of porous ceramics will be a benefit for the pollutant diffusion and transfer, and at least 0.6 MPa of compressive strength was considered as a desirable value for porous TiO_2 ceramic to resist the hydraulic blow. In addition, from the mercury porosimetry test (Figure S7, Supporting Information), the pore size distribution of W15 was 1.06 μm, suggesting its macropores existence, and this result was also in agreement with the SEM observation. The apparent density of W15 was 0.7633 kg/m^3. Comparing with Figure S6 (Supporting Information), 21 nm of the pore size distribution could be observed for W15, implying its aggregated mesopores existence.

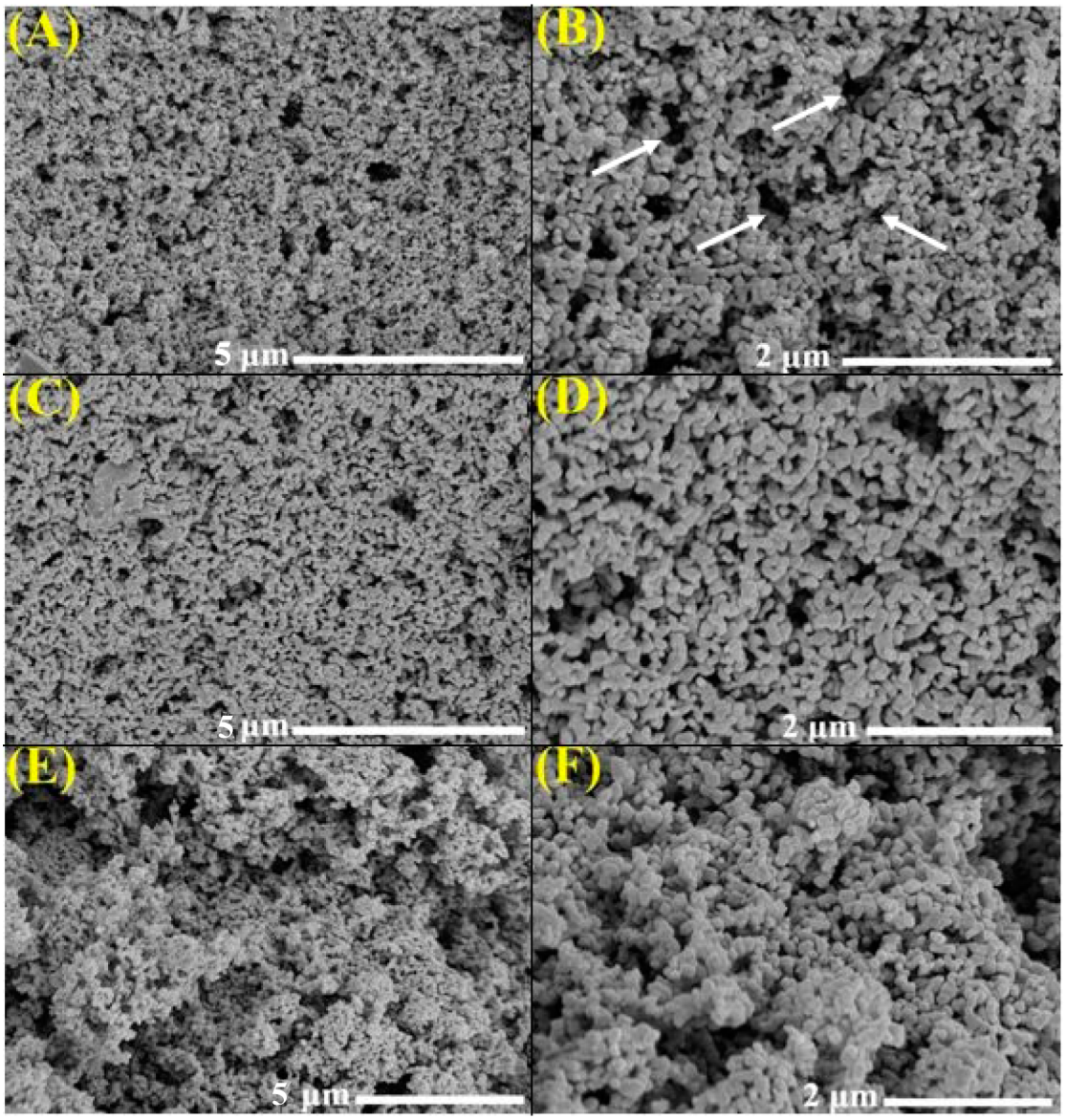

Figure 3. SEM images of the calcined samples at 800 °C from (A, B) 10 wt %, (C, D) 15 wt %, and (E, F) 20 wt % TiO_2 solid content slurries.

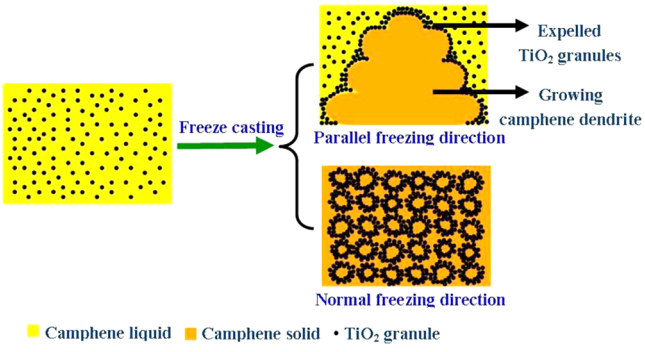

Figure 4. Schematic diagram for the in situ formation of porous TiO_2 ceramic by the freeze-drying of TiO_2 ceramic slurry.

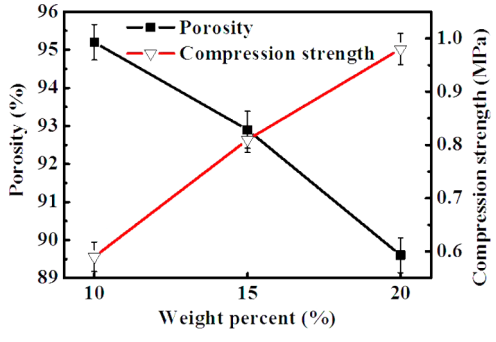

Figure 5. Porosity and compressive strength of porous TiO_2 ceramics prepared with 10, 15, and 20 wt % TiO_2 solid content slurries, respectively.

Therefore, the prepared TiO_2 ceramic possessed the hierarchical porous structure. With 15 wt % TiO_2 solid content at 800 °C calcinations, high porosity and mechanical strength of porous TiO_2 ceramic could be achieved. In addition, it could still achieve suppression of TiO_2 anatase-to-rutile phase transformation, high crystallinity, relative large specific surface area, and small TiO_2 grain size at 800 °C calcinations by XRD, TEM, SEM, and BET characterization. These results would favor the photocatalytic performance of floating porous TiO_2 ceramics photocatalyst.

dx.doi.org/10.1021/am5034236 | ACS Appl. Mater. Interfaces 2014, 6, 16653−16660

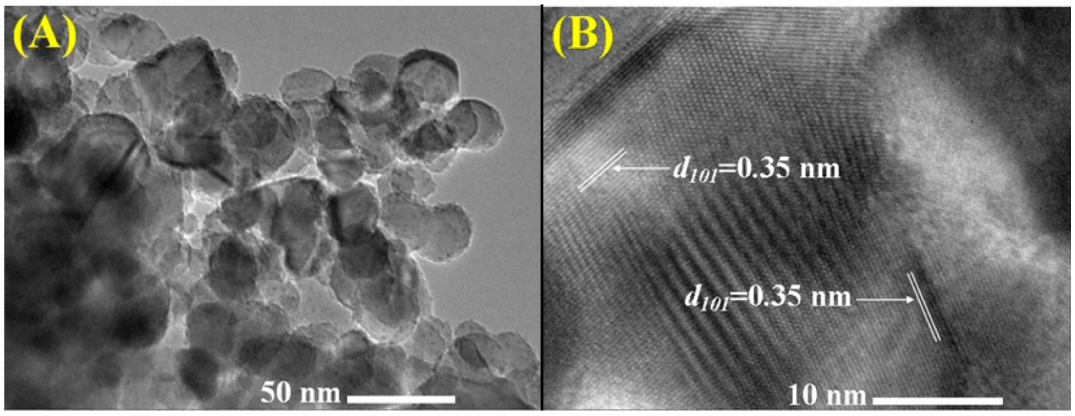

Figure 6. (A) TEM and (B) HRTEM images of porous TiO_2 ceramics prepared with 15 wt % TiO_2 solid content slurries at 800 °C. (anatase: d_{101} = 0.35 nm).

The morphology and porosity of porous TiO_2 ceramic was further analyzed by TEM. Figure 6 showed the TEM and high-resolution TEM (HRTEM) images of prepared porous TiO_2 ceramic with 15 wt % TiO_2 solid content after 800 °C calcinations. From Figure 6A, the average 20−30 nm of TiO_2 particles was observed, which was in agreement with the XRD and SEM analyses. Moreover, the TiO_2 particles would adhere to each other and form a porous structure by accumulating these particles. From the HRTEM image (Figure 6B), the lattice fringes indexed to the (101) (d_{101} = 0.35 nm) crystal face of anatase, which was also consistent with the XRD analysis.

3.2. Photocatalytic Testing for Pesticide Micropolluted Water Degradation. In order to better know the link between the TiO_2 solid content and photocatalytic activity, the photocatalytic performance of W10, W15, and W20 on atrazine degradation was examined. As shown in Figure 7, the atrazine

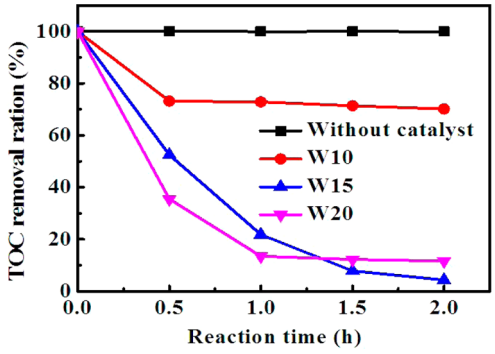

Figure 7. Effect of TiO_2 solid content on the photocatalytic degradation of atrazine within 2 h irradiation.

TOC degradation rate of W15 excelled that of W10 and W20. W15 achieved the highest atrazine TOC degradation rate (95.7%) after 2 h reaction. However, W10 and W20 removed only 29.9% and 88.4% of atrazine after 2 h reaction. When the solid content was at 10 wt %, the prepared porous TiO_2 ceramic began to easily disintegrate in water after 0.5 h illumination. However, when the TiO_2 solid content reached 20 wt %, the more TiO_2 powders added caused the floating capability of porous TiO_2 ceramic to decline significantly after 1 h illumination; therefore, 15 wt % TiO_2 solid content was determined as the optimal condition for the fabrication of high efficient and durable floating porous TiO_2 ceramic photocatalysts. The reason was the fact that W15 could obtain high porosity, high mechanical strength, and high photocatalytic activity. Moreover, the atrazine concentration remained invariable for 2 h with the UV lamp alone, suggesting that UV photolysis could not degrade atrazine directly. With 2 h of dark adsorption testing, the initial atrazine concentration also kept invariable, demonstrating that the adsorption capability of the porous TiO_2 ceramic was not obvious. Therefore, the main atrazine degradation mechanism was photocatalysis.

To further inspect the porous TiO_2 ceramic activity, the 5 mg/L soluble thiobencarb removal was also examined by W10, W15, and W20. In Figure 8, after 2 h photocatalysis, W15

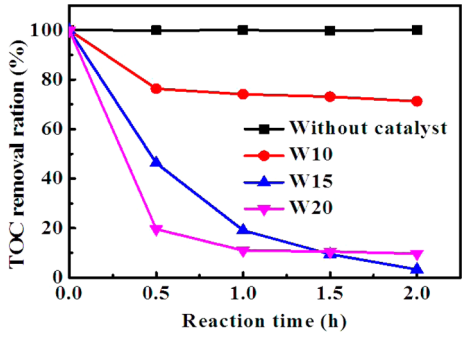

Figure 8. Effect of TiO_2 solid content on the photocatalytic degradation of thiobencarb within 2 h irradiation.

achieved the highest thiobencarb TOC removal ratio of 96.7%. However, W10 and W20 removed only 28.8% and 90.4% of thiobencarb. In terms of the photocatalytic efficiency, the W15 excelled that of W10 and W20. Moreover, the thiobencarb concentration remained invariable for 2 h with the UV lamp alone, suggesting that UV photolysis also could not degrade thiobencarb directly. With 2 h of dark adsorption testing, the initial thiobencarb concentration also kept invariable, demonstrating that the adsorption capability of the porous TiO_2 ceramic was poor. These results were well consistent with atrazine removal.

An obvious advantage of porous TiO_2 ceramic is its high recycling stability. So, its photocatalytic performance during multiple cycling was also tested. Figure 9 showed the photocatalytic removal of atrazine and thiobencarb with porous TiO_2 ceramics over six cycles. All higher than 95% of atrazine and thiobencarb TOC removal was obtained within 2 h of irradiation per cycle. Therefore, our prepared porous TiO_2

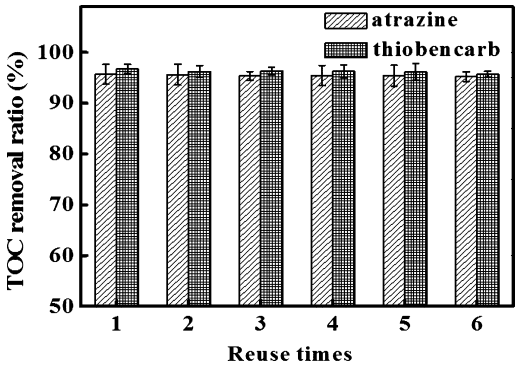

Figure 9. Effect of porous TiO_2 ceramic recycling on 5 mg/L atrazine and thiobencarb photodegradation by W15.

ceramics were both easily reused and retained high photocatalytic performance during recycling. As a contrast with W15, the same weight of P25 powders was examined in the same photocatalytic conditions for the atrazine and thiobencarb degradation. Only 19% and 20% of TOC removal efficiencies could be obtained after 2 h irradiation, respectively. With nonstirred reactions, most P25 powders sank to the bottom of the reactor, and a small amount of P25 powders was suspended in the solution that increased the turbidity of water. On the one hand, the muddy water blocked the contact between light and bottom TiO_2 powder. On the other hand, without the aeration condition, the dissolved oxygen was difficult to participate in the photocatalytic reaction process. Together this demonstrated that the atrazine and thiobencarb degradation for floating porous TiO_2 ceramic was clearly better than that of P25 powders. For the P25 powder recycles and water purge, centrifugation or a filtration process had to be used with high energy consumption. This further suggested that the floating TiO_2 ceramics were far superior to traditional TiO_2 powder for industrial catalyst recycling.

Moreover, besides atrazine and thiobencarb, the photodegradation of other types of pesticide contaminants was also inspected, including 5 mg/L dimethoate, lindane, dipterex, malathion, and bentazone. Figure 10 indicated that a TOC

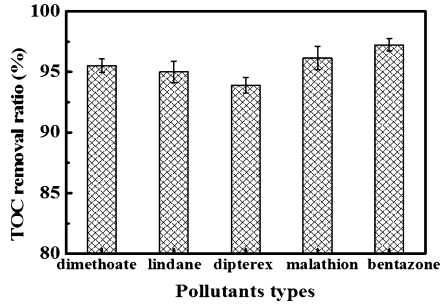

Figure 10. Effect of floating photocatalysts on the TOC removal of 5 mg/L pollutants by W15.

removal efficiency of 95.5%, 95.0%, 93.9%, 96.1%, and 97.2% could be achieved after 2 h photocatalysis for dimethoate, lindane, dipterex, malathion, and bentazone, respectively. These results suggested that the synthesized porous TiO_2 ceramic had the universality for multiple pesticide micropolluted water degradation.

4. CONCLUSIONS

A lightweight floating porous TiO_2 ceramic photocatalyst was successfully synthesized through a camphene-based freeze-drying route. The TiO_2 solid content was a key parameter to determine the pore structure, mechanical resistance, and photocatalytic activity of porous TiO_2 ceramic. With the TiO_2 solid content adjusting from 10 to 20 wt %, the porosity reduced from 95.2% to 89.6%, and the compressive strength raised from 0.59 to 0.98 MPa. TiO_2 solid content also can affect the photocatalytic activity of the samples significantly. A solid content of 15 wt % was confirmed as the optimal solid content for the fabrication of high efficient and durable floating TiO_2 ceramic photocatalyst. The TOC removal efficiency for atrazine and thiobencarb was 95.7% and 96.7% after irradiation for 2 h, respectively. Furthermore, the floating photocatalyst could be recycling several times with no obvious decline in the atrazine and thiobencarb TOC removal. Dimethoate, lindane, dipterex, malathion, and bentazone could also be degraded effectively using the porous TiO_2 ceramic without any oxygenation or stirring. Therefore, the obtained floating photocatalyst has the potential to exploit solar energy at the water surface for the cleanup of refractory pesticide micropollutants in natural or industrial water environment in the future.

■ ASSOCIATED CONTENT

Ⓢ Supporting Information

Schematic chart of the fabrication procedure; figure of the change of the relative weight during freeze-drying of camphene-based green body, TGA analyses of the dispersant, TGA analyses of the binder, and TGA analyses of the green body after the freeze-drying; image of floating porous TiO_2 ceramic; images of the vertical and lateral views of floating porous TiO_2 ceramic with single ceramic; schematic representation of a floating porous TiO_2 ceramic for contaminant oxidation; nitrogen adsorption−desorption isotherms and the pore size distribution (insert) of the materials synthesized; and the pore size distribution of porous TiO_2 ceramics. This material is available free of charge via the Internet at http://pubs.acs.org.

■ AUTHOR INFORMATION

Corresponding Authors

*(W.Z.) E-mail: zwmater@gmail.com.
*(W.L.) E-mail: li_w10@fudan.edu.cn.

Notes

The authors declare no competing financial interest.

■ ACKNOWLEDGMENTS

We gratefully acknowledge the support of this research by the National Natural Science Foundation of China (21376065, 81302511, 21106035, and 21101060), the Natural Science Foundation of Heilongjiang Province (QC2012C001, QC2013C079, and QC2012C046), the Program for New Century Excellent Talents in University of Heilongjiang Province (1253-NCET-020), the Scientific Research Fund of Heilongjiang Provincial Education Department (12521226), the Special Fund of Technological Innovation Talents in Harbin City (2013RFQXJ002), and the Heilongjiang University Excellent Youth Foundation (JCL201102).

■ REFERENCES

(1) Mitsika, E. E.; Christophoros, C.; Fytianos, K. Fenton and Fenton-like Oxidation of Pesticide Acetamiprid in Water Samples:

Kinetic Study of the Degradation and Optimization Using Response Surface Methodology. *Chemosphere* **2013**, *93*, 1818−1825.
(2) Sanches, S.; Penetra, A.; Rodrigues, A.; Cardoso, V. V.; Ferreira, E.; Benoliel, M. J.; Crespo, M. T. B.; Crespo, J. G.; Pereira, V. J. Removal of Pesticides from Water Combining Low Pressure UV Photolysis with Nanofiltration. *Sep. Purif. Technol.* **2013**, *115*, 73−82.
(3) Xing, Z.; Sun, D.; Yu, X.; Zou, J.; Zhou, W. Treatment of Antibiotic Fermentation-Based Pharmaceutical Wastewater Using Anaerobic and Aerobic Moving Bed Bioflim Reactors Combined with Ozone/hydrogen Peroxide Process. *Environ. Prog. Sustainable Energy* **2014**, *33*, 170−177.
(4) Shannon, M. A.; Bohn, P. W.; Elimelech, M.; Georgiadis, J. G.; Mariñas, B. J.; Mayes, A. M. Science and Technology for Water Purification in the Coming Decades. *Nature* **2008**, *452*, 301−310.
(5) Marino, T.; Molinari, R.; García, H. Selectivity of Gold Nanoparticles on the Photocatalytic Activity of TiO_2 for the Hydroxylation of Benzene by Water. *Catal. Today* **2013**, *206*, 40−45.
(6) Daghrir, R.; Drogui, P.; Robert, D. Modified TiO_2 for Environmental Photocatalytic Applications: A Review. *Ind. Eng. Chem. Res.* **2013**, *52*, 3581−3599.
(7) Bai, H.; Liu, Z.; Liu, L.; Sun, D. D. Large-Scale Production of Hierarchical TiO_2 Nanorod Spheres for Photocatalytic Elimination of Contaminants and Killing Bacteria. *Chem.—Eur. J.* **2013**, *19*, 3061−3070.
(8) Wu, Q.; Zhao, J.; Qin, G.; Wang, C.; Tong, X.; Xue, S. Photocatalytic Reduction of Cr(VI) with TiO_2 Film under Visible Light. *Appl. Catal., B* **2013**, *142−143*, 142−148.
(9) Sheng, H.; Li, Q.; Ma, W.; Ji, H.; Chen, C.; Zhao, J. Photocatalytic Degradation of Organic Pollutants on Surface Anionized TiO_2: Common Effect of Anions for High Hole-Availability by Water. *Appl. Catal., B* **2013**, *138−139*, 212−218.
(10) Chen, D.; Zhang, H.; Liu, Y.; Li, J. H. Graphene and Its Derivatives for the Development of Solar Cells, Photoelectrochemical, and Photocatalytic Applications. *Energy Environ. Sci.* **2013**, *6*, 1362−1387.
(11) Kubacka, A.; García, M. F.; Colón, G. Advanced Nanoarchitectures for Solar Photocatalytic Applications. *Chem. Rev.* **2012**, *112*, 1555−1614.
(12) Baniasadi, E.; Dincer, I.; Naterer, G. F. Hybrid Photocatalytic Water Splitting for an Expanded Range of the Solar Spectrum with Cadmium Sulfide and Zinc Sulfide Catalysts. *Appl. Catal., A* **2013**, *455*, 25−31.
(13) Kibombo, H. S.; Koodali, R. T. Heterogeneous Photocatalytic Remediation of Phenol by Platinized Titania-Silica Mixed Oxides under Solar-Simulated Conditions. *J. Phys. Chem. C* **2011**, *115*, 25568−25579.
(14) Chaleshtori, M. Z.; Hosseini, M.; Edalatpour, R.; Masud, S. M. S.; Chianelli, R. R. Photocatalytic Decontamination of Wastewater with Porous Material HNb_3O_8. *Microchem. J.* **2013**, *110*, 361−368.
(15) Xing, Z.; Zhou, W.; Du, F.; Qu, Y.; Tian, G.; Pan, K.; Tian, C.; Fu, H. A Foating Macro/Mesoporous Crystalline Anatase TiO_2 Ceramic with Enhanced Photocatalytic Performance for Recalcitrant Wastewater Degradation. *Dalton Trans.* **2014**, *43*, 790−798.
(16) Ye, J.; Liu, W.; Cai, J.; Chen, S.; Zhao, X.; Zhou, H.; Qi, L. Nanoporous Anatase TiO_2 Mesocrystals: Additive-Free Synthesis, Remarkable Crystalline-Phase Stability, and Improved Lithium Insertion Behavior. *J. Am. Chem. Soc.* **2011**, *133*, 933−940.
(17) Joo, J. B.; Zhang, Q.; Lee, I.; Dahl, M.; Zaera, F.; Yin, Y. Mesoporous Anatase Titania Hollow Nanostructures though Silica-Protected Calcination. *Adv. Funct. Mater.* **2012**, *22*, 166−174.
(18) Miao, G.; Chen, L.; Qi, Z. Facile Synthesis and Active Photocatalysis of Mesoporous and Microporous TiO_2 Nanoparticles. *Eur. J. Inorg. Chem.* **2012**, *2012*, 5864−5871.
(19) Bian, Z.; Tachikawa, T.; Zhang, P.; Fujitsuka, M.; Majima, T. A Nanocomposite Superstructure of Metal Oxides with Effective Charge Transfer Interfaces. *Nat. Commun.* **2014**, *5*, 3038.
(20) Li, X.; Liu, J.; Masters, A. F.; Pareek, V. K.; Maschmeyer, T. Hollow Micro/nanomaterials as Nanoreactors for Photocatalysis. *APL Mater.* **2013**, *1*, 041101.
(21) Etacheri, V.; Seery, M. K.; Hinder, S. J.; Pillai, S. C. Oxygen Rich Titania: A Dopant Free, High Temperature Stable, and Visible-Light Active Anatase Photocatalyst. *Adv. Funct. Mater.* **2011**, *21*, 3744−3752.
(22) Cheng, X.; Yu, X.; Xing, Z. One-Step Synthesis of Visible Active CNS-Tridoped TiO_2 Photocatalyst from Biomolecule Cystine. *Appl. Surf. Sci.* **2012**, *258*, 7644−7650.
(23) Kachina, A.; Puzenat, E.; Ould-Chikh, S.; Geantet, C.; Delichere, P.; Afanasiev, P. A New Approach to the Preparation of Nitrogen-Doped Titania Visible Light Photocatalyst. *Chem. Mater.* **2012**, *24*, 636−642.
(24) Bian, Z.; Tachikawa, T.; Zhang, P.; Fujitsuka, M.; Majima, T. Au/TiO_2 Superstructure-Based Plasmonic Photocatalysts Exhibiting Efficient Charge Separation and Unprecedented Activity. *J. Am. Chem. Soc.* **2014**, *136*, 458−465.
(25) Lin, Y.; Geng, Z.; Cai, H.; Ma, L.; Chen, J.; Zeng, J.; Pan, N.; Wang, X. Ternary Graphene-TiO_2-Fe_3O_4 Nanocomposite as a Recollectable Photocatalyst with Enhanced Durability. *Eur. J. Inorg. Chem.* **2012**, *2012*, 4439−4444.
(26) Zhang, G.; Yi, J.; Shim, J.; Lee, J.; Choi, W. Photocatalytic Hydroxylation of Benzene to Phenol over Titanium Oxide Entrapped into Hydrophobically Modified Siliceous Foam. *Appl. Catal., B* **2011**, *102*, 132−139.
(27) Rey, A.; Quiñones, D. H.; Álvarez, P. M.; Beltrán, F. J.; Plucinski, P. K. Simulated Solar-Light Assisted Photocatalytic Ozonation of Metoprolol over Titania-Coated Magnetic Activated Carbon. *Appl. Catal., B* **2012**, *111*, 246−253.
(28) Aziz, A. A.; Yong, K. S.; Ibrahim, S.; Pichiah, S. Enhanced Magnetic Separation and Photocatalytic Activity of Nitrogen Doped Titania Photocatalyst Supported on Strontium Ferrite. *J. Hazard. Mater.* **2012**, *199*, 143−150.
(29) Crick, C. R.; Bear, J. C.; Kafizas, A.; Parkin, I. P. Superhydrophobic Photocatalytic Surfaces through Direct Incorporation of Titania Nanoparticles into a Polymer Matrix by Aerosol Assisted Chemical Vapor Deposition. *Adv. Mater.* **2012**, *24*, 3505−3508.
(30) Han, H.; Bai, R. Buoyant Photocatalyst with Greatly Enhanced Visible-Light Activity Prepared through a Low Temperature Hydrothermal Method. *Ind. Eng. Chem. Res.* **2009**, *48*, 2891−2898.
(31) Fabiyi, M. E.; Skelton, R. L. Photocatalytic Mineralization of Methylene Blue Using Buoyant TiO_2-Coated Polystyrene Beads. *J. Photochem. Photobiol., A* **2000**, *132*, 121−128.
(32) Hosseini, S. N.; Borghei, S. M.; Vossoughi, M.; Taghavinia, N. Immobilization of TiO_2 on Perlite Granules for Photocatalytic Degradation of Phenol. *Appl. Catal., B* **2007**, *74*, 53−62.
(33) Modestov, A.; Glezer, V.; Marjasin, I.; Lev, O. Photocatalytic Degradation of Chlorinated Phenoxyacetic Acids by a New Buoyant Titania-Exfoliated Graphite Composite Photocatalyst. *J. Phys. Chem. B* **1997**, *101*, 4623−4629.
(34) Magalhães, F.; Lago, R. M. Floating Photocatalysts Based on TiO_2 Grafted on Expanded Polystyrene Beads for the Solar Degradation of Dyes. *Sol. Energy* **2009**, *83*, 1521−1526.
(35) Koh, Y. H.; Lee, E. J.; Yoon, B. H.; Song, J. H.; Kim, H. E. Effect of Polystyrene Addition on Freeze Casting of Ceramic/Camphene Slurry for Ultra-high Porosity Ceramics with Aligned Pore Channels. *J. Am. Ceram. Soc.* **2006**, *89*, 3646−3653.
(36) Soon, Y. M.; Shin, K. H.; Koh, Y. H.; Lee, J. H.; Kim, H. E. Compressive Strength and Processing of Camphene-Based Freeze Cast Calcium Phosphate Scaffolds with Aligned Pores. *Mater. Lett.* **2009**, *63*, 1548−1550.
(37) Liu, H.; Chen, S.; Wang, G.; Qiao, S. Z. Ordered Mesoporous Core/Shell SnO_2/C Nanocomposite as High Capacity Anode Material for Lithium Ion Battery. *Chem.—Eur. J.* **2013**, *19*, 16897−16901.
(38) Liu, J.; Yang, T.; Wang, D. W.; Lu, G. Q.; Zhao, D.; Qiao, S. Z. A Facile Soft-Template Synthesis of Mesoporous Polymeric and Carbonaceous Nanospheres. *Nat. Commun.* **2013**, *4*, 2798.
(39) Liu, H.; Du, X.; Xing, X.; Wang, G.; Qiao, S. Z. Highly Ordered Mesoporous Cr_2O_3 Materials with Enhanced Performance for Gas Sensors and Lithium Ion Batteries. *Chem. Commun.* **2012**, *48*, 865−867.

(40) Hong, C.; Du, J.; Liang, J.; Zhang, X.; Han, J. Functionally Graded Porous Ceramics with Dense Surface Layer Produced by Freeze-Casting. *Ceram. Int.* **2011**, *37*, 3717−3722.
(41) Ren, L.; Zeng, Y. P.; Jiang, D. Fabrication of Gradient Pore TiO_2 Sheets by a Novel Freeze−Tape-Casting Process. *J. Am. Ceram. Soc.* **2007**, *90*, 3001−3004.
(42) Chen, R.; Wang, C. A.; Huang, Y.; Ma, L.; Lin, W. Ceramics with Special Porous Structures Fabricated by Freeze-Gelcasting: Using tert-Butyl Alcohol as a Template. *J. Am. Ceram. Soc.* **2007**, *90*, 3478−3484.
(43) Araki, K.; Halloran, J. W. New Freeze-Casting Technique for Ceramics with Sublimable Vehicles. *J. Am. Ceram. Soc.* **2004**, *87*, 1859−1863.
(44) Araki, K.; Halloran, J. W. Room-Temperature Freeze Casting for Ceramics with Nonaqueous Sublimable Vehicles in the Naphthalene−Camphor Eutectic System. *J. Am. Ceram. Soc.* **2004**, *87*, 2014−2019.
(45) Tian, G.; Fu, H.; Jing, L.; Xin, B.; Pan, K. Preparation and Characterization of Stable Biphase TiO_2 Photocatalyst with High Crystallinity, Large Surface Area, and Enhanced Photoactivity. *J. Phys. Chem. C* **2008**, *112*, 3083−3089.
(46) Zhou, W.; Sun, F.; Pan, K.; Tian, G.; Jiang, B.; Ren, Z.; Tian, C.; Fu, H. Well-Ordered Large-Pore Mesoporous Anatase TiO_2 with Remarkably High Thermal Stability and Improved Crystallinity: Preparation, Characterization, and Photocatalytic Performance. *Adv. Funct. Mater.* **2011**, *21*, 1922−1930.
(47) Xing, Z.; Li, J.; Wang, Q.; Zhou, W.; Tian, G.; Pan, K.; Tian, C.; Zou, J.; Fu, H. A Floating Porous Crystalline TiO_2 Ceramic with Enhanced Photocatalytic Performance for Wastewater Decontamination. *Eur. J. Inorg. Chem.* **2013**, *2013*, 2411−2417.
(48) American Public Health Association. *Standard Methods for the Examination of Water and Wastewater*, 20th ed.; APHA: New York, 1998.
(49) Yang, Q.; Li, M.; Liu, J.; Shen, W.; Ye, C.; Shi, X.; Jiang, L.; Song, Y. Hierarchical TiO_2 Photonic Crystal Spheres Prepared by Spray Drying for Highly Efficient Photocatalysis. *J. Mater. Chem. A* **2013**, *1*, 541−547.
(50) Fernández-García, M.; Martínez-Arias, A.; Hanson, J. C.; Rodriguez, J. A. Nanostructured Oxides in Chemistry: Characterization and Properties. *Chem. Rev.* **2004**, *104*, 4063−4104.
(51) Nalan, N. T.; Seery, M. K.; Hinder, S. J.; Healy, L. F.; Pillai, S. C. A Systematic Study of the Effect of Silver on the Chelation of Formic Acid to a Titanium Precursor and the Resulting Effect on the Anatase to Rutile Transformation of TiO_2. *J. Phys. Chem. C* **2010**, *114*, 13026−13034.
(52) Zhou, W.; Fu, H. Mesoporous TiO_2: Preparation, Doping, and as a Composite for Photocatalysis. *ChemCatChem.* **2013**, *5*, 885−894.
(53) Djafer, L.; Ayral, A.; Boury, B.; Laine, R. M. Surface Modification of Titania Powder P25 with Phosphate and Phosphonic Acids-Effect on Thermal Stability and Photocatalytic Activity. *J. Colloid Interface Sci.* **2013**, *393*, 335−339.
(54) Jing, L.; Zhou, W.; Tian, G.; Fu, H. Surface Tuning for Oxide-Based Nanomaterials as Efficient Photocatalysts. *Chem. Soc. Rev.* **2013**, *42*, 9509−9549.